Journal of Luminescence 202 (2018) 316–321

Contents lists available at ScienceDirect

Journal of Luminescence

journal homepage: www.elsevier.com/locate/jlumin

Analysis of the upconversion emission of yttrium orthoaluminate nano-perovskite co-doped with Er^{3+}/Yb^{3+} ions for thermal sensing applications

M.A. Hernández-Rodriguez[a,*], A.D. Lozano-Gorrín[a], V. Lavín[a], U.R. Rodríguez-Mendoza[a], I.R. Martín[a], F.J. Manjón[b]

[a] Departamento de Física, MALTA Consolider Team, IUdEA and IMN, Universidad de La Laguna, Apdo. 456, E-38200 San Cristóbal de La Laguna, Santa Cruz de Tenerife, Spain

[b] Instituto de Diseño para la Fabricación y Producción Automatizada, MALTA Consolider Team, Universitat Politécnica de València, Cno. de Vera s/n, 46022 Valencia, Spain

ABSTRACT

The upconversion emissions of yttrium orthoaluminate nano-perovskite co-doped with Er^{3+}/Yb^{3+} have been studied. Strong green and red upconversion emissions, which can be observed by naked eyes, were observed when exciting the sample at 980 nm. In particular, the green band was monitored as a function of temperature and the obtained results suggest that this nano-perovskite can be used as an optical temperature sensor by exciting in the infrared range. The viability of YAP:Er^{3+}/Yb^{3+} nano-perovskite in laser heating applications has been tested and discussed.

1. Introduction

Lanthanide doped materials have been extensively researched due to their applications in several fields, for instance, laser materials [1–5], bio-imaging [6–11], optoelectronic [12,13] and optical temperature sensors [14–22]. Special attention has been paid to the down- and up-conversion (UC) emission properties of the Erbium trivalent ion (Er^{3+}) [23]. Moreover, several studies revealed that Er^{3+}-based ferroelectrics present excellent electrical and luminescence properties [24]. Nonetheless, the low absorption of Er^{3+} around 980 nm yield a low emission efficiency that limits the practical application of this ion in commercial devices. Fortunately, Ytterbium trivalent ion (Yb^{3+}) presents a strong and broad absorption band ranging from 850 to 1050 nm [21] and a good energy transfer (ETU) from Yb^{3+} to Er^{3+} [25]. Therefore, host co-doping with Er^{3+}/Yb^{3+} is very interesting for practical applications because Yb^{3+} can be used as an excellent sensitizer in highly luminescent Er^{3+}-doped materials.

Another issue which has drawn much attention in the last years is the research on optical thermal sensors based on UC emissions of materials and nanomaterials doped with lanthanide ions. For instance, nano-phosphors [26,27] and $NaYF_4$:Er^{3+}/Yb^{3+} nanoparticles can be used a nano-thermometer with high temperature resolution [28], while $NaNbO_3$:Yb^{3+}/Tm^{3+} nanocrystals and Y_2O_3:Yb^{3+}/Ho^{3+} nanopowders can be used as optical thermal sensors [29,30].

In this sense, the research on nanomaterials has become an important issue to concern, due to the outstanding properties of these materials [31]. Among nanomaterials hosts, yttrium orthoaluminate nano-perovskite (YAP) can be a good candidate due to its excellent chemical stability and mechanical and thermal properties [32]. In order to explore the combination of the excellent mechanical-chemical properties of YAP nano-perovskite with the high UC emission efficiency of Er^{3+} ions, enhanced by Yb^{3+} ions as Er^{3+} sensitizers, we study in this work the viability of YAP nano-perovskite co-doped with 2.5 mol% of Yb^{3+}/Er^{3+} as an optical temperature sensor and its potential use in laser heating applications.

2. Experimental details

YAP nano-perovskite of composition $Y_{(1-x-y)}Er_xYb_yAlO_3$, with x = 0.025 and y = 0.025 (in mol%) (YAP:Er^{3+}/Yb^{3+} from now) was successfully synthesized by the sol–gel method in an air atmosphere. Stoichiometric molar ratios of high-purity $Y(NO_3)_3{\cdot}4H_2O$ (ALDRICH, 99.9%), $Al(NO_3)_3{\cdot}9H_2O$ (ALDRICH, 99.9%), $Er(NO_3)_3{\cdot}5H_2O$ (ALDRICH, 99.9%) and $Yb(NO_3)_3{\cdot}5H_2O$ (ALDRICH, 99.9%) materials were dissolved in 25 ml of 1 M HNO_3 under stirring at 353 K for 3 h. Then citric acid, with a molar ratio of metal ions to citric acid of 1:2, was added to the solution, which was stirred and heated at 363 K until the solution becomes transparent. Subsequently, 4 mg of polyethylene glycol was added to the solution to form a gel. This gel was fired at 400 °C for 6 h to remove the residual nitrates and organic compounds and get the

* Corresponding author.
E-mail address: miguelandreshr@gmail.com (M.A. Hernández-Rodriguez).

https://doi.org/10.1016/j.jlumin.2018.05.078
Received 25 November 2017; Received in revised form 11 May 2018; Accepted 31 May 2018
Available online 01 June 2018
0022-2313/

powder sample. This powder was initially burnt out at 1200 °C for 20 h in a first thermal treatment and then at 1550 °C for 12 h in a second thermal treatment. The object of the thermal treatments is to achieve the orthorhombic structure of the $YAlO_3$ (more details about this in Ref. [33]). Powder X-ray diffraction data were collected on a PANalytical X'Pert PRO diffractometer (Bragg-Brentano geometry) with an X'Celerator detector employing the Cu $K\alpha_1$ radiation ($\lambda = 1.5405$ Å) in the angular range $5° < 2\theta < 80°$, by continuous scanning with a step size of 0.02°. On the other hand, the luminescence measurements from RT to 600 K were carried out in a tubular electric furnace where the samples were placed at the center of it and heated at a rate of 1.25 K/min. The temperature of the sample was controlled with a type K thermocouple in contact with it and connected to a voltmeter (Fluke Calibrator 714). A 980 nm commercial laser with a maximum power of 343 mW excited the sample from one side of the furnace, while the emission was collimated by a lens located on the other exit side, and then focalized with a another lens into an optical fiber coupled to a 0.5 m single grating spectrometer (Andor SR-500i-B2-R). The laser spot size on the sample (defined as the $1/e^2$ radius of the intensity) was shown to be 5.6 μm of diameter. Detection of luminescence signal was carried out with a cooled CCD detector (Newton DU490A-1.7) with a resolution of 0.7 nm ($\sim 25\ cm^{-1}$) and an integration time of 1 s. The luminescence decay curves were measured by exciting the sample with a pulsed parametric oscillator OPO (EKSPLA/NT342/3/UVE) laser and using an analogic storage oscilloscope (LeCroy WS424) coupled to the detection system. All spectra were corrected for the spectral response of the equipment.

3. Fluorescence intensity ratio technique

The fluorescence intensity ratio (FIR) technique was used in the second part of this work in order to calibrate the YAP:Er^{3+}/Yb^{3+} nano-perovskite emission with the temperature. In this technique, the fluorescence intensity of two nearby levels, i.e. $^2H_{11/2}$ and $^4S_{3/2}$ levels of Er^{3+} levels, is registered as a function of temperature and interpreted in terms of a simple three-level scheme system (see Fig. 1). Since the energy gap of this pair of thermalized levels is very small, the population of the upper level from the lower level is allowed by thermal excitation. The issue here is that the ratio of these intensities is independent of the laser source, because the emitted intensities only depend on the population proportionality of the involved levels. Thus, the relationship between the relative population of the thermalized levels, R, and the temperature can be described by the Boltzmann's distribution law by the equation:

$$R = \frac{I_{31}}{I_{21}} = \frac{\omega_{31}^R g_3 h\nu_3}{\omega_{21}^R g_2 h\nu_2} e^{-E_{32}/kT} = Ce^{-E_{32}/kT} \quad (1)$$

where k is the Boltzmann constant, E_{32} is the energy gap between the pair of thermalized levels, g_3, g_2 are the degeneracies $(2J + 1)$, I_{31}, I_{21} are the integrated intensities of the thermalized levels, ω_{31}^R and ω_{21}^R are the spontaneous emission rates of the E_3 and E_2 levels to the E_1 level, respectively.

The sensor relative sensitivity S_{REL} is defined as follows:

$$S_{REL} = \frac{1}{R}\left|\frac{dR}{dT}\right| = \left(\frac{E_{32}}{kT^2}\right) \quad (2)$$

The sensor relative sensitivity S_{REL} permits the comparison of the sensitivity with other optical temperature sensor ones, because it only depends on the temperature. It is evident that a larger energy gap between the thermalized levels, leads to a higher sensitivity. However, larger energy gap also means lower population in the upper thermalized level and thus, lower intensity.

The main of FIR technique for temperature sensing is that it neglects accuracy problems resulting from fluctuations of the excitation or from the lack of absolute emission intensities which could occur by noise in the detection system.

Concerning the temperature uncertainty, δT, it is known that this magnitude is the smallest temperature change (temperature resolution) that can be achieved in a given measurement and can be calculated by the equation [34]:

$$\delta T = \frac{1}{S_{REL}}\frac{\delta R}{R} \quad (3)$$

where S_{REL} is the relative sensitivity and the $\delta R/R$ is the relative uncertainty on R.

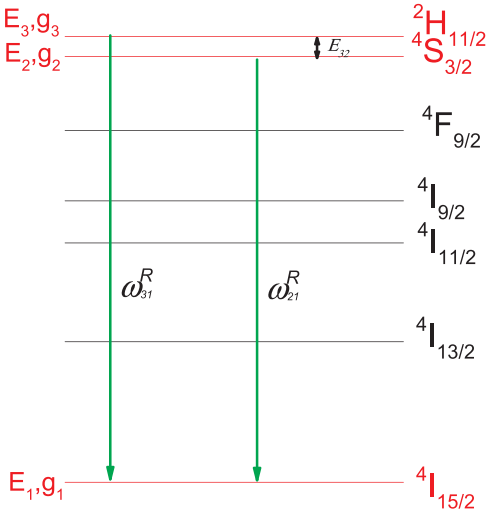

Fig. 1. Simplified diagram for three level system applied on the Er^{3+} ion energy level scheme. E_{32} is the energy gap between the two excited levels, g_i is the degeneracy of the i-th level and ω_{ij}^R is the spontaneous emission rate between the i-th and j-th levels.

4. Results and discussion

4.1. Structural characterization

X-ray diffraction spectrum of YAP:Er^{3+}/Yb^{3+} is depicted in Fig. 2. The XRD pattern of the YAP:Er^{3+}/Yb^{3+} nano-perovskite was indexed to an orthorhombic structure space group *Pnma* phase. Hence, XRD confirms the perovskite-type structure of YAP:Er^{3+}/Yb^{3+}. Unit cell of YAP:Er^{3+}/Yb^{3+} nano-perovskite is also given in Fig. 2. Crystal structure parameters have been obtained from fitting process of the profiles of the nano-perovskites by the Rietveld method using FULLPROF

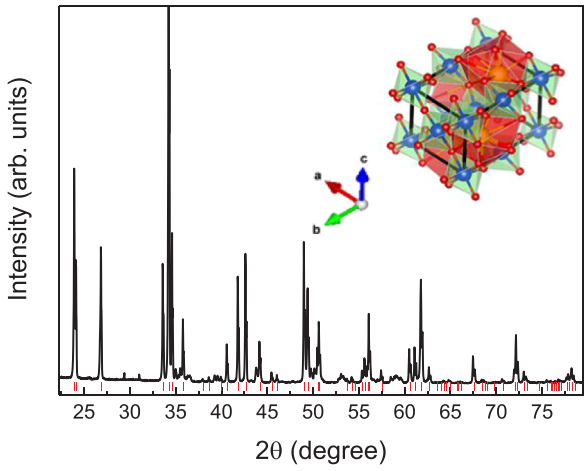

Fig. 2. XRD patterns of the YAP:Er^{3+}/Yb^{3+} nano-perovskite and the corresponding *Pnma* symmetry Rietveld refinement at ambient conditions. The unit cell is also shown.

Table 1
Cell parameters and reliability factors obtained from fitting of XRD pattern for YAP:Er^{3+}/Yb^{3+}.

a (Å)	*b* (Å)	*c* (Å)	V (Å^3)	χ^2	R_p	R_{wp}	R_{exp}
5.323(1)	7.364(1)	5.174(1)	202.8(1)	4.95	24.3	29.5	17.1

program [35] (see Table 1).

The average grains size "*D*" was determined from Scherrer formula:

$$D = \frac{0.89\lambda}{\beta \, \mathrm{Cos}\, \theta} \quad (4)$$

where λ = 1.5406 Å, β is the full width at half maximum of the peaks and θ is the angle of diffraction. The average grains size value was around 35–40 nm. No amorphous phase was detected in the nano-perovskite sample.

4.2. Upconversion mechanism

Under 980 nm excitation and ambient conditions, YAP:Er^{3+}/Yb^{3+} nano-perovskite shows a strong UC emission which can be observed by naked eye as well (see Fig. 3). The UC spectrum can be divided in two parts, the first one is attributed to the green emissions assigned to ($^2H_{11/2}$, $^4S_{3/2}$)→$^2I_{15/2}$ transitions and the second one is attributed to the red emission related to the $^4F_{9/2}$→$^2I_{15/2}$ transition.

To understand the physical mechanism responsible for the UC process in YAP:Er^{3+}/Yb^{3+} nano-perovskite, the dependence of the UC emissions with the pump power was analyzed. It is known that the number of photons, *n*, which are needed to populate the upper emitting state can be estimated by the formula:

$$I_{UC} \propto I_{Pump}^{n} \quad (5)$$

where I_{UC} is the intensity of the UC band emission, I_{Pump} is the pump power of the excitation source. Increasing the pump power of the 980 nm laser source, it can be observed that the UC emission intensities increase with the pump power (see Fig. 4(a)). The *n* values of YAP:Er^{3+}/Yb^{3+} nano-perovskite for the green (550 nm) and red (660 nm) emission bands are 1.77 and 1.76 respectively, as shown in Fig. 4(b). This result suggests that a two-photon process is involved in both the population of $^4S_{3/2}$ and $^4F_{9/2}$ levels.

The temporal evolution of the UC intensities at 550 nm and 660 nm are shown in Fig. 5. The rise time that can be seen in both curves indicates that the UC mechanism is based on energy transfer processes (ETU) in which an excited ion transfers its energy to a neighbor excited ion, which is promoted to a higher excited state. Otherwise, when the rise time is negligible, then the UC processes are due to an excited state absorption mechanism (ESA) that involves the absorption of a photon by a unique ion that promotes to a higher excited state.

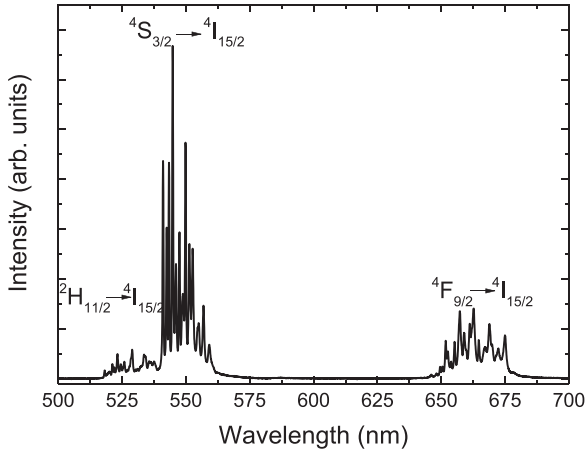

Fig. 3. UC emission spectrum of YAP:Er^{3+}/Yb^{3+} nano-perovskite obtained at ambient conditions under 980 nm excitation.

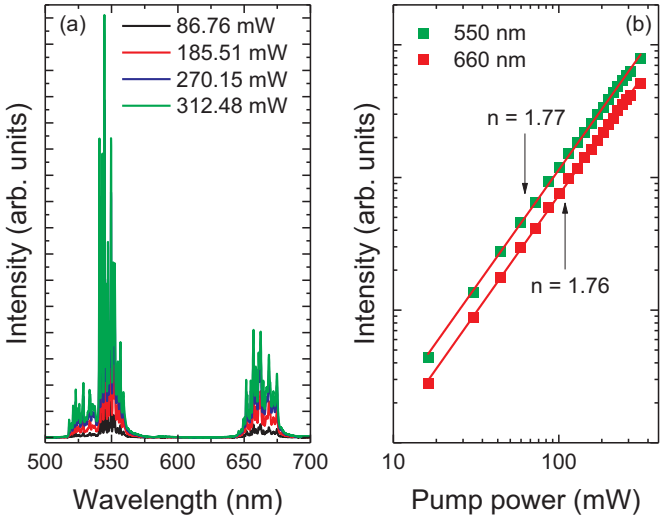

Fig. 4. (a) UC emission spectra of YAP:Er^{3+}/Yb^{3+} under different pump powers at ambient conditions and (b) UC intensities of YAP:Er^{3+}/Yb^{3+} nano-perovskite as functions of the pump power at 980 nm in a double-log scale. Linear fit dependences give slopes of 1.77 and 1.76 for the 550 nm and 660 nm bands, respectively.

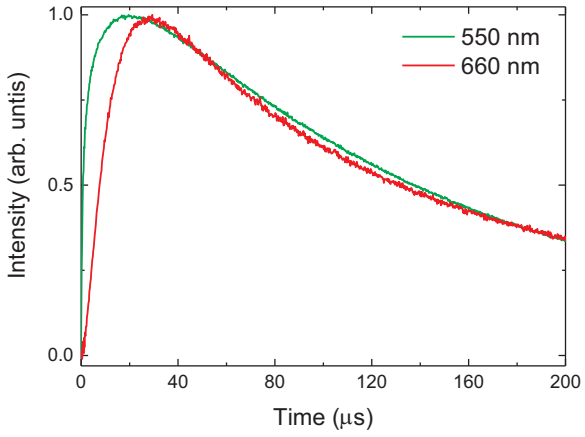

Fig. 5. Temporal evolutions of the UC emissions of YAP:Er^{3+}/Yb^{3+} nano-perovskite at 550 nm and 660 nm under excitation at 980 nm.

Based on the results shown in Figs. 4 and 5, it can be confirmed that the mechanism behind the UC emission is an ETU process with different steps. The simplified energy level diagram of YAP:Er^{3+}/Yb^{3+} nano-perovskite is depicted in Fig. 6. The UC mechanism for YAP:Er^{3+}/Yb^{3+} nano-perovskite is the energy transfer ETU from Yb^{3+} to Er^{3+} ions. Exciting at 980 nm, Yb^{3+} ions in the ground level promote to the $^2F_{5/2}$ level by ground state absorption (GSA) and then, the energy of these ions is transferred to Er^{3+} ions. Afterwards, electrons that are coming from Er^{3+} ions are excited to the $^4I_{11/2}$ level and partly decay to the $^4I_{13/2}$ level by multiphonon relaxation (MPR) processes. At this stage, a second energy photon can be absorbed by Yb^{3+} ions and transferred to Er^{3+} ions again, during the lifetime of the $^4I_{11/2}$ and $^4I_{13/2}$ levels. This leads to the population $^4F_{7/2}$ and $^4F_{9/2}$ levels from the excitation of the electrons that come from $^4I_{11/2}$ and $^4I_{13/2}$ levels, respectively. Then, these electrons decay to the $^2H_{11/2}$, $^4S_{3/2}$ and $^4F_{9/2}$ levels via MPR process. Finally, a radiative transition process occurs leading to the green and red emissions related to the ($^2H_{11/2}$, $^4S_{3/2}$) → $^2I_{15/2}$ and $^4F_{9/2}$→ $^2I_{15/2}$ transitions, respectively.

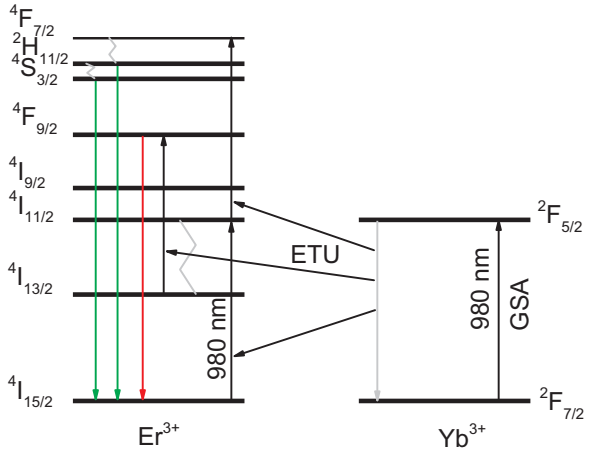

Fig. 6. Partial energy level diagram of YAP:Er^{3+}/Yb^{3+} nano-perovskite under 980 nm excitation and possible UC processes.

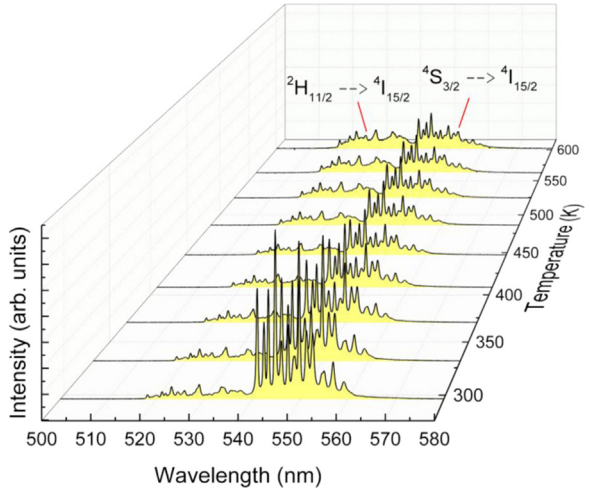

Fig. 7. Temperature evolution of the upconversion emission of the YAP:Er^{3+}/Yb^{3+} nano-perovskite.

4.3. Optical sensor calibration

Since YAP:Er^{3+}/Yb^{3+} nano-perovskite shows strong UC emission intensities, its viability as optical thermal sensor was analyzed.

The temperature evolution of the YAP:Er^{3+}/Yb^{3+} nano-perovskite UC emission spectra from room temperature up to 600 K are shown in Fig. 7. It can be observed that the emission band associated with the $^4S_{3/2} \rightarrow {}^4I_{15/2}$ (550 nm) transition was decreasing as the temperature increases, while the emission band associated with the $^2H_{11/2} \rightarrow {}^4I_{15/2}$ (530 nm) transition was increasing, because of the thermally induced population that comes from the $^4S_{3/2}$ level.

An analysis based on a simple three-level system scheme formed by $^2H_{11/2}$ (level 3), $^4S_{3/2}$ (level 2) and $^4I_{15/2}$ (level 1) was performed. The ratio between the integrated intensities for $^2H_{11/2} \rightarrow {}^4I_{15/2}$ and $^4S_{3/2} \rightarrow {}^4I_{15/2}$ was increasing with the temperature, following a tendency that can be described by Eq. (1). From the fitting process, the values of $C = 5.77$ and the energy gap $E_{32} = 751.10\,cm^{-1}$ have been determinate. The relative sensor sensitivity S_{REL} as a function of the temperature T, defined by the Eq. (2) is also shown in Fig. 8. The temperature uncertainty δT achieved in the optical calibration procedure is also shown in Fig. 8.

The maximum relative sensitivity achieved for YAP:Er^{3+}/Yb^{3+} nano-perovskite was $0.0123\,K^{-1}$ with a temperature uncertainty around of 0.42 K. The relative sensitivity of YAP:Er^{3+}/Yb^{3+} nano-perovskite was compared with others RE^{3+}- based temperature optical sensors (see Table 2). YAP:Er^{3+}/Yb^{3+} shows a very high sensitivity, and thus, it can be considered as potential candidate to become an optical temperature sensor based on the FIR technique working in the VIS range exciting in NIR.

4.4. Laser heating application

Taking advantage of the temperature calibration of the YAP:Er^{3+}/Yb^{3+} performed in the previous section of this work, it is possible to obtain the temperature heating of the 980 nm laser source. The increment of temperature and ratio as a function of the pump power of the laser source are shown in Fig. 9. As can be observed, it is possible to heat the nano-perovskite sample and control its temperature with the laser power. Therefore, with a pump power of 350 mW it is possible to increase its temperature 100 K with an uncertainty lower than 1 K in this temperature range (according to Fig. 8b).

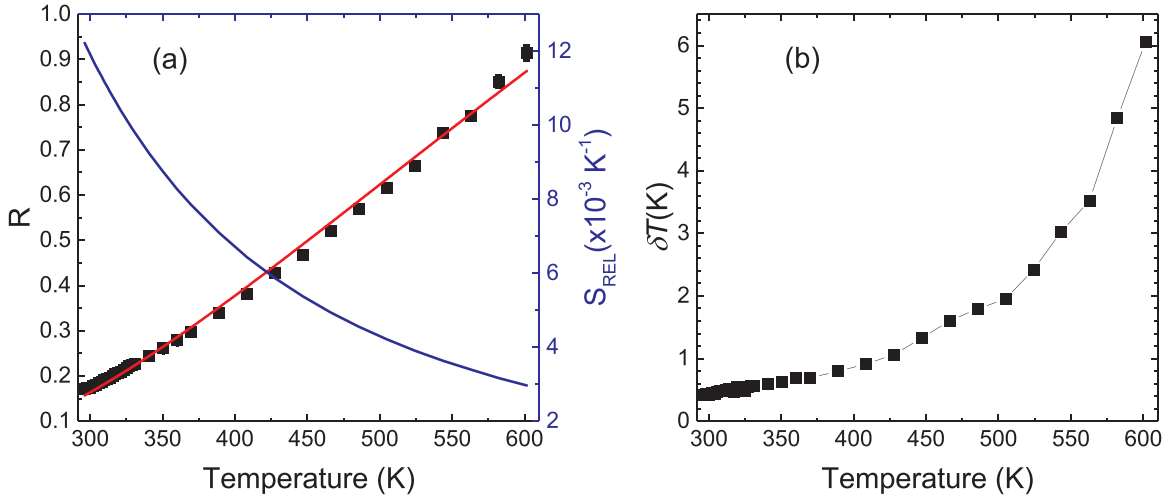

Fig. 8. (a) Experimental integrated intensity ratio (R) (black squares) and relative sensitivity (S_{REL}) (blue line) of the YAP:Er^{3+}/Yb^{3+}nano-perovskite obtained from the emission bands associated to the $^2H_{11/2} \rightarrow {}^4I_{15/2}$ and $^4S_{3/2} \rightarrow {}^4I_{15/2}$ transitions. The experimental values were fitted to Eq. (1) (red line). (b) Temperature uncertainty δT computed by Eq. (3).

Table 2
Thermal relative sensitivity at 296 K of different RE^{3+}- based temperature optical sensors[a].

Er^{3+}/Yb^{3+} doped host material	FIR equation	Transition	Temperature range (K)	λ_{EXC} (nm)	S_{REL} (x10^{-3} K^{-1}) at 300 K	Ref.
$NaBiTO_3:Er^{3+}/Yb^{3+}$ ceramic	9.77•exp(− 795/kT)	$(^2H_{11/2}, {}^4S_{3/2}) \rightarrow {}^4I_{15/2}$	200–443	980	12.6	[24]
YAP:Er^{3+}/Yb^{3+} nano-perovskite	5.77•exp(− 751.10/kT)	$(^2H_{11/2}, {}^4S_{3/2}) \rightarrow {}^4I_{15/2}$	296–600	980	11.9	This work
$NaYF_4:Er^{3+}$ nano-crystalline	10•exp(− 741/kT)	$(^2H_{11/2}, {}^4S_{3/2}) \rightarrow {}^4I_{15/2}$	294–720	488	11.7	[19]
Lanthanum Oxysulfide powder:Er^{3+}	8.75•exp(− 712.57/kT)	$(^2H_{11/2}, {}^4S_{3/2}) \rightarrow {}^4I_{15/2}$	240–300	806	11.3	[20]
$Al_2O_3:Er^{3+}/Yb^{3+}$ nano-particles	9.63•exp(− 674/kT)	$(^2H_{11/2}, {}^4S_{3/2}) \rightarrow {}^4I_{15/2}$	295–975	978	10.6	[23]
$Na_{0.5}Bi_{0.5}TiO_3:Er^{3+}/Yb^{3+}$ ceramic	4.71•exp(− 579.10/kT)	$(^2H_{11/2}, {}^4S_{3/2}) \rightarrow {}^4I_{15/2}$	93–613	980	9.2	[36]
Chalcogenide glass: Er^{3+}/Yb^{3+}	5.98•exp(− 555/kT)	$(^2H_{11/2}, {}^4S_{3/2}) \rightarrow {}^4I_{15/2}$	293–493	1060	8.8	[37]
$Na_2Y_2B_2O_7:Er^{3+}/Yb^{3+}$ nano-phosphor	27.6•exp(− 536.40/kT)	$(^2H_{11/2}, {}^4S_{3/2}) \rightarrow {}^4I_{15/2}$	300–613	980	8.5	[26]
Silicate glass: Er^{3+}/Yb^{3+}	3.65•exp(− 414.80/kT)	$(^2H_{11/2}, {}^4S_{3/2}) \rightarrow {}^4I_{15/2}$	296–723	978	6.6	[38]
$CaMoO_4:Er^{3+}/Yb^{3+}$ nano-phosphor	5.10•exp(− 379.40/kT)	$(^2H_{11/2}, {}^4S_{3/2}) \rightarrow {}^4I_{15/2}$	300–535	980	6	[27]

[a] FIR Equations, transitions of interest, relative sensibilities as well as the temperature ranges and excitation wavelengths are also included.

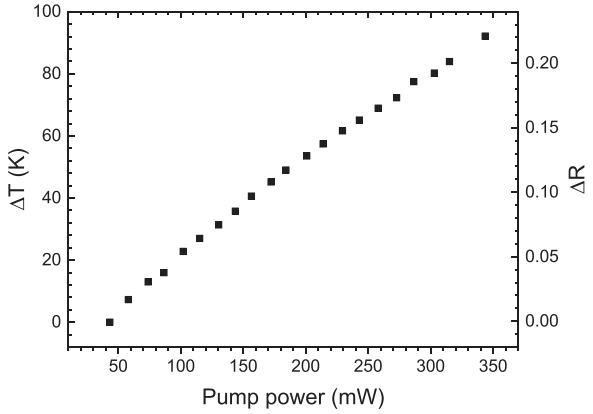

Fig. 9. Temperature and ratio increments as functions of the pump power of the laser source.

5. Conclusions

Upconversion properties of YAP:Er^{3+}/Yb^{3+} nano-perovskite exciting at 980 nm have been analyzed. Under 980 nm excitation, the green UC emissions at 530 nm ($^2H_{11/2} \rightarrow {}^4I_{15/2}$) and 550 nm ($^4S_{3/2} \rightarrow {}^4I_{15/2}$) as a function of temperature from RT to 600 K were studied. The obtained results show a high sensitivity in YAP:Er^{3+}/Yb^{3+} nano-perovskite (0.0123 K^{-1} with a temperature uncertainty around of 0.42 K) which is better than many other optical temperature sensors based on Er^{3+} and Er^{3+}/Yb^{3+}, suggesting its viability as optical temperature sensor based on the FIR technique working in the VIS range exciting in NIR. The temperature of the YAP:Er^{3+}/Yb^{3+} nano-perovskite can be controlled by heating with the pump power of the excitation laser, suggesting its potential viability in laser heating applications.

Acknowledgements

This research was partially supported MINECO (MAT2013-46649-C4-2/4-P, MAT2015-71070-REDC, and MAT2016-75586-C4-2/4-P), and by the EU-FEDER. M.A. Hernández-Rodríguez thanks to MINECO for FPI grant (BES-2014-068666).

References

[1] J.J. Romero, E. Montoya, L.E. Bausá, F. Agulló-Rueda, M.R.B. Andreeta, A.C. Hernandes, Multiwavelength laser action of Nd^{3+}:$YAlO_3$ single crystals grown by the laser heated pedestal growth method, Opt. Mater. 24 (2004) 643–650, http://dx.doi.org/10.1016/S0925-3467(03)00179-4.

[2] M. Bass, Nd,Cr : "$YAlO_3$ laser tailored for high-energy Q-switched operation", Appl. Phys. Lett. 17 (1970) 395–398, http://dx.doi.org/10.1063/1.1653451.

[3] I. Iparraguirre, J. Azkargorta, J.M. Fernández-Navarro, M. Al-Saleh, J. Fernández, R. Balda, Laser action and upconversion of Nd^{3+} in tellurite bulk glass, J. Non Cryst. Solids 353 (2007) 990–992, http://dx.doi.org/10.1016/j.jnoncrysol.2006.12.103.

[4] M.J. Weber, M. Bass, T.E. Varitimos, D.P. Bua, Laser action from Ho^{3+}, Er^{3+}, and Tm^{3+} in $YAlO_3$, IEEE J. Quantum Electron. QE-9 (1973) 1079–1086, http://dx.doi.org/10.1109/JQE.1973.1077426.

[5] M.J. Weber, M. Bass, K. Andringa, R.R. Monchamp, E. Comperch, Czochralski growth and properties of $YAlO_3$ laser crystals, Appl. Phys. Lett. 15 (1969) 342–345, http://dx.doi.org/10.1063/1.1652851.

[6] D. Jaque, F. Vetrone, Luminescence nanothermometry, Nanoscale 4 (2012) 4301–4326, http://dx.doi.org/10.1039/c2nr30764b.

[7] S. Xu, S. Huang, Q. He, L. Wang, Upconversion nanophosphores for bioimaging, Trends Anal. Chem. 66 (2015) 72–79, http://dx.doi.org/10.1016/j.trac.2014.11.014.

[8] U. Rocha, K.U. Kumar, C. Jacinto, I. Villa, F. Sanz-Rodríguez, M. Del Carmen Iglesias De La Cruz, A. Juarranz, E. Carrasco, F.C.J.M. Van Veggel, E. Bovero, J.G. Solé, D. Jaque, Neodymium-doped LaF_3 nanoparticles for fluorescence bioimaging in the second biological window, Small 10 (2014) 1141–1154, http://dx.doi.org/10.1002/smll.201301716.

[9] D. Wawrzynczyk, A. Bednarkiewicz, M. Nyk, W. Strek, M. Samoc, Neodymium(iii) doped fluoride nanoparticles as non-contact optical temperature sensors, Nanoscale 4 (2012) 6959, http://dx.doi.org/10.1039/c2nr32203j.

[10] H. Söderlund, S. Andersson-engels, Increasing depth penetration in biological tissue imaging using 808-nm upconverting nanoparticles, J. Biomed. Opt. 20 (2015) 086008–0860014, http://dx.doi.org/10.1117/1.JBO.20.8.086008.

[11] U. Rocha, C. Jacinto Da Silva, W. Ferreira Silva, I. Guedes, A. Benayas, L. Martínez Maestro, M. Acosta Elias, E. Bovero, F.C.J.M. Van Veggel, J.A. García Solé, D. Jaque, Subtissue thermal sensing based on neodymium-doped LaF_3 nanoparticles, ACS Nano 7 (2013) 1188–1199, http://dx.doi.org/10.1021/nn304373q.

[12] H. Wang, Y. Liu, M. Li, H. Huang, H.M. Xu, R.J. Hong, H. Shen, Multifunctional TiO_2 nanowires-modified nanoparticles bilayer film for 3D dye-sensitized solar cells, Optoelectron. Adv. Mater. Rapid Commun. 4 (2010) 1166–1169, http://dx.doi.org/10.1039/b000000x.

[13] F. Zhang, G.B. Braun, Y. Shi, Y. Zhang, X. Sun, N.O. Reich, D. Zhao, G. Stucky, J. Hao, L.H. Fischer, G.S. Harms, O.S. Wolfbeis, Z.L. Wang, J. Hao, H.L.W. Chan, W.T. Wong, K.L. Wong, Metal-ion doped luminescent thin films for optoelectronic applications, J. Mater. Chem. C 8 (2013) 2850–2851, http://dx.doi.org/10.1002/smll.201102703.

[14] X. Wang, J. Zheng, Y. Xuan, X. Yan, Optical temperature sensing of $NaYbF_4$:Tm^{3+}@SiO_2 core-shell micro-particles induced by infrared excitation, Opt. Express 21 (2013) 21596–21606, http://dx.doi.org/10.1364/OE.21.021596.

[15] H. Zou, X. Wang, Y. Hu, X. Zhu, Y. Sui, Z. Song, Optical temperature sensing by upconversion luminescence of Er doped $Bi_5TiNbWO_{15}$ ferroelectric materials, AIP Adv. 4 (2014) 1–7, http://dx.doi.org/10.1063/1.4905454.

[16] L. Xing, Y. Xu, R. Wang, W. Xu, Z. Zhang, Highly sensitive optical thermometry based on upconversion emissions in Tm^{3+}/Yb^{3+} codoped $LiNbO_3$ single crystal, Opt. Lett. 39 (2014) 454–457, http://dx.doi.org/10.1364/OL.39.000454.

[17] E.A. Lalla, S.F. León-Luis, V. Monteseguro, C. Pérez-Rodríguez, J.M. Cáceres, V. Lavín, U.R. Rodríguez-Mendoza, Optical temperature sensor based on the Nd^{3+} infrared thermalized emissions in a fluorotellurite glass, J. Lumin. 166 (2015) 209–214, http://dx.doi.org/10.1016/j.jlumin.2015.05.029.

[18] R. Dey, A. Kumari, A.K. Soni, V.K. Rai, $CaMoO_4$:Ho^{3+}-Yb^{3+}-Mg^{2+} upconverting phosphor for application in lighting devices and optical temperature sensing, Sens. Actuators B Chem. 210 (2015), pp. 581–588, http://dx.doi.org/10.1016/j.snb.2015.01.007.

[19] A. Benayas, B. Del Rosal, A. Pérez-Delgado, K. Santacruz-Gómez, D. Jaque, G.A. Hirata, F. Vetrone, Nd:YAG Near-infrared luminescent nanothermometers, Adv. Opt. Mater 3 (2015), pp. 687–694, http://dx.doi.org/10.1002/adom.201400484.

[20] S. Wang, H. Zhou, X. Wang, A. Pan, Up-conversion luminescence and optical temperature-sensing properties of Er^{3+}-doped perovskite $Na_{0.5}Bi_{0.5}TiO_3$ nanocrystals, J. Phys. Chem. Solids 98 (2016) 28–31, http://dx.doi.org/10.1016/j.jpcs.2016.06.002.

[21] M.A. Hernández-Rodríguez, A.D. Lozano-Gorrín, I.R. Martín, U.R. Rodríguez-Mendoza, V. Lavín, Comparison of the sensitivity as optical temperature sensor of nano-perovskite doped with Nd^{3+} ions in the first and second biological windows, Sens. Actuators B Chem. 255 (2018) 970–976, http://dx.doi.org/10.1016/j.snb.2017.08.140.

[22] M.A. Hernández-Rodríguez, A.D. Lozano-Gorrín, V. Lavín, U.R. Rodríguez-Mendoza, I.R. Martín, Yttrium orthoaluminate nanoperovskite doped with Tm^{3+} ions as upconversion optical temperature sensor in the near-infrared region, Opt. Express 25 (2017) 27845–27856, http://dx.doi.org/10.1364/OE.25.027845.

[23] P. Du, L. Luo, W. Li, Y. Zhang, H. Chen, Electrical and luminescence properties of Er-doped $Bi_{0.5}Na_{0.5}TiO_3$ ceramics, Mater. Sci. Eng. B 178 (2013) 1219–1223, http://dx.doi.org/10.1016/j.mseb.2013.08.007.

[24] P. Du, L. Luo, W. Li, Q. Yue, H. Chen, Optical temperature sensor based on up-conversion emission in Er-doped ferroelectric $0.5Ba(Zr_{0.2}Ti_{0.8})O_3$-$0.5(Ba_{0.7}Ca_{0.3})TiO_3$ ceramic, Appl. Phys. Lett. 104 (2014) 2–6, http://dx.doi.org/10.1063/1.4871378.

[25] L.H. Fischer, G.S. Harms, O.S. Wolfbeis, Upconverting nanoparticles for nanoscale thermometry, Angew. Chem. - Int. Ed. 50 (2011) 4546–4551, http://dx.doi.org/10.1002/anie.201006835.

[26] A.K. Soni, V.K. Rai, M.K. Mahata, Yb^{3+} sensitized $Na_2Y_2B_2O_7$:Er^{3+} phosphors in enhanced frequency upconversion, temperature sensing and field emission display, Elsevier Ltd, 2017, http://dx.doi.org/10.1016/j.materresbull.2017.01.009.

[27] S. Sinha, M.K. Mahata, K. Kumar, S.P. Tiwari, V.K. Rai, Dualistic temperature sensing in Er^{3+}/Yb^{3+} doped $CaMoO_4$ upconversion phosphor, SAA (2016), http://dx.doi.org/10.1016/j.saa.2016.09.039.

[28] F. Vetrone, R. Naccache, A. Zamarrón, A.J. De. La Fuente, F. Sanz-Rodríguez, L.M. Maestro, E.M. Rodriguez, D. Jaque, J.G. Sole, J.A. Capobianco, Temperature sensing using fluorescent nanothermometers, ACS Nano 4 (2010) 3254–3258, http://dx.doi.org/10.1021/nn100244a.

[29] A.F. Pereira, K.U. Kumar, W.F. Silva, W.Q. Santos, D. Jaque, C. Jacinto, Yb^{3+}/Tm^{3+} co-doped $NaNbO_3$ nanocrystals as three-photon-excited luminescent nanothermometers, Sens. Actuators B Chem. 213 (2015) 65–71, http://dx.doi.org/10.1016/j.snb.2015.01.136.

[30] V. Lojpur, M. Nikolic, L. Mancic, O. Milosevic, M.D. Dramicanin, Y_2O_3:Yb,Tm and Y_2O_3:Yb,Ho powders for low-temperature thermometry based on up-conversion fluorescence, Ceram. Int. 39 (2013) 1129–1134, http://dx.doi.org/10.1016/j.ceramint.2012.07.036.

[31] E. Roduner, Size matters: why nanomaterials are different, Chem. Soc. Rev. 35 (2006) 583–592, http://dx.doi.org/10.1039/b502142c.

[32] R. Moncorgé, B. Chambon, J.Y. Rivoire, N. Garnier, E. Descroix, P. Laporte, H. Guillet, S. Roy, J. Mareschal, D. Pelenc, J. Doury, P. Farge, Nd doped crystals for medical laser applications, Opt. Mater. 8 (1997) 109–119, http://dx.doi.org/10.1016/S0925-3467(97)00022-0.

[33] C.D.S. Brites, A. Milla, Lanthanides in luminescent thermometry, Handb. Phys. Chem. Rare Earths 49 (2016), http://dx.doi.org/10.1016/bs.hpcre.2016.03.005.

[34] J. Rodríguez-Carvajal, Recent advances in magnetic structure determination by neutron powder diffraction, Phys. B Condens. Matter 192 (1993) 55–69, http://dx.doi.org/10.1016/0921-4526(93)90108-I.

[35] M.A. Hernández-Rodríguez, A.D. Lozano-Gorrín, I.R. Martín, U.R. Rodríguez-Mendoza, V. Lavín, Spectroscopic properties of Nd^{3+} ions in YAP nano-perovskites, J. Lumin. 188 (2017) 204–208, http://dx.doi.org/10.1016/j.jlumin.2017.04.031.

[36] P. Du, L. Luo, W. Li, Q. Yue, Upconversion emission in Er-doped and Er/Yb-codoped ferroelectric $Na_{0.5}Bi_{0.5}TiO_3$ and its temperature sensing application, J. Alloy. Compd. 116 (2014) 014102–014107, http://dx.doi.org/10.1063/1.4886575.

[37] P.V. Santos, M.T. De Araujo, J.A.M. Neto, A.S.B. Sombra, Optical thermometry through infrared excited upconversion fluorescence emission in Er - and Er – Yb -doped chalcogenide glasses, Quantum 35 (1999) 395–399, http://dx.doi.org/10.1109/3.748846.

[38] X. Wang, X. Yan, Ultraviolet and infrared photon-excited synergistic effect in Er^{3+}-doped YbF_3 phosphors, Opt. Lett. 36 (2011) 4353–4355, http://dx.doi.org/10.1364/OL.36.004353.